Optical properties of nanocrystalline diamond thin films

P. Achatz, J. A. Garrido, M. Stutzmann, O. A. Williams, D. M. Gruen, A. Kromka, and D. Steinmüller

Citation: Applied Physics Letters **88**, 101908 (2006); doi: 10.1063/1.2183366
View online: http://dx.doi.org/10.1063/1.2183366
View Table of Contents: http://scitation.aip.org/content/aip/journal/apl/88/10?ver=pdfcov
Published by the AIP Publishing

Optical properties of nanocrystalline diamond thin films

P. Achatz, J. A. Garrido,[a] and M. Stutzmann
Walter Schottky Institut, Technische Universität München, Am Coulombwall, D-85748 Garching, Germany

O. A. Williams
Institute for Materials Research, Universiteit Hasselt, Wetenschapspark 1, 3590 Diepenbeek, Belgium

D. M. Gruen
Materials Science Division, Argonne National Laboratory, Argonne, Illinois 60439

A. Kromka and D. Steinmüller
ρ-BeSt coating GmbH, A-6150 Steinach, Austria

(Received 21 July 2005; accepted 26 January 2006; published online 8 March 2006)

The optical properties of nanocrystalline diamond films grown from a hydrogen-rich CH_4/H_2 gas phase by hot filament chemical vapor deposition, as well as from an argon-rich Ar/CH_4 gas phase by microwave plasma enhanced chemical vapor deposition, are reported. The influence of nitrogen incorporation on the optical absorption is investigated. The diamond films are characterized by photothermal deflection spectroscopy and temperature dependent spectrally resolved photoconductivity. An onset of absorption at about 0.8 eV in undoped films is attributed to transitions from π to π states introduced into the band gap by the high amount of sp^2 bonded carbon at the grain boundaries. Incorporation of nitrogen leads to a strong absorption in the whole energy spectrum, as a result of the increasing number of sp^2 carbon atoms. The effect of surface states has been observed in the high energy region of the spectrum. Transitions to the conduction band tail and photothermal ionization processes account for the observed onset at 4.4 eV. Photocurrent quenching at about 3.3 eV is observed in the case of samples grown from a hydrogen-rich CH_4/H_2 gas phase. © *2006 American Institute of Physics*. [DOI: 10.1063/1.2183366]

Nanocrystalline diamond thin films recently have attracted renewed interest, mainly due to the appearance of a very high *n*-type conductivity induced by the addition of nitrogen during growth. It has been shown that ultrananocrystalline diamond films can be deposited over large areas with a surface roughness down to 10 nm.[1] Thus, nanocrystalline diamond has been proposed as particularly adequate for tribological applications such as microelectromechanical systems,[2] or biomedical implants requiring high wear resistance and biocompatibility.[3]

While the sp^3 phase of the diamond grains (grain size in the nanometer range) influences its mechanical properties, the sp^2-bonded carbon atoms in the grain boundaries control the films' electronic and optical properties. The influence of π states in the grain boundaries on the electronic band structure have been studied theoretically using a tight-binding model based on high-angle high-energy twist grain boundaries.[4] Recently the electronic properties have been examined on the basis of the electronic structure of amorphous carbon.[5] Both theoretical and experimental results suggest that conduction occurs in the grain boundaries, most probably by hopping and impurity band conduction. The main effect of nitrogen is to increase the density of states associated with sp^2-bonded carbon atoms. In this letter, photothermal deflection spectroscopy (PDS) and spectrally resolved photoconductivity (SPC) have been applied to obtain further information about the sub-band gap structure of nanocrystalline diamond films.

Two kind of samples (about 1 μm thick) have been investigated. Nanocrystalline diamond films were grown on quartz in a microwave plasma chemical vapor deposition process from an argon-rich $Ar/N_2/CH_4$ gas phase. The CH_4 flow rate was kept constant at 1.4 sccm, while the flow rate of N_2 and Ar was varied to maintain a 100 sccm total flow rate. The substrate temperature was maintained at 800 °C, while the total pressure and input power were kept at 100 Torr and 1200 W, respectively. The samples are designated by a "R", N_2 (vol %) refers to the amount of nitrogen in the gas phase. Sample R0 shows a conductivity of about 1×10^{-6} Ω^{-1} cm^{-1}, whereas sample R5 already shows a conductivity of 8 Ω^{-1} cm^{-1}. On the other hand, nanocrystalline diamond samples were grown on quartz from a hydrogen-rich CH_4/H_2 gas phase via hot filament CVD. The flow rate of H_2 and CH_4 was maintained at 99 and 1 sccm, respectively. The substrate temperature was kept constant at 700 °C. These samples are designated with "AAu". PDS and SPC measurements show similar results for both types of samples, indicating the existence of a common nanocrystalline diamond phase. The thickness of the samples is about 1 μm.

Figure 1(a) shows the schematic band structure of undoped nanocrystalline diamond. Theoretical models predict the presence of π and π^* states in the band gap of diamond, placed symmetrically around the Fermi energy.[4] This is quite similar to amorphous carbon[6] and CVD diamond.[7] Nitrogen incorporation causes a significant increase and broadening of the π and π^* bands. The disorder in the grain boundaries results in a reduction of the energy gap due to band tailing. So-called σ^* states are introduced into the forbidden gap by

[a]Electronic mail: garrido@wsi.tum.de

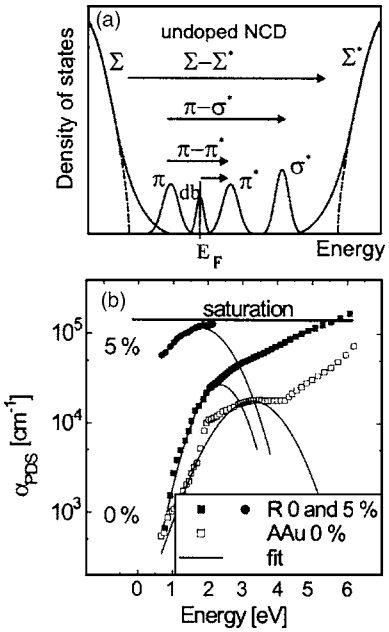

FIG. 1. (a) π and π^* states introduced by sp^2 bonded carbon atoms, dangling bond (db) states, as well as disorder induced band tailing (Σ,Σ^*) dominate the band structure of undoped nanocrystalline diamond, σ^* states refer to distorted tetrahedrally bonded carbon atoms in the grain boundary. (b) Absorption coefficient measured with PDS for samples R0, R5, and AAu.

the distortion of sp^3 bonds, as well as dangling bond states.[4]

The optical absorption coefficient α measured with PDS of samples AAu, R0, and R5 is shown in Fig. 1(b). The optical absorption spectra of the undoped samples have a sharp onset at about 0.8 eV and increase steadily with increasing excitation energy. Sample R5 grown from an argon-rich microwave plasma with 5% N_2 in the gas shows a much more pronounced π-π^* component. The onset of optical absorption is shifted to lower energies. α values above the saturation level of PDS of 10^5 cm^{-1} cannot be determined any more with reasonable accuracy. Samples with still higher nitrogen content (not shown) exhibit saturation of the absorption over the whole spectral range.

The onset at about 0.8 eV in the absorption spectra is attributed to transitions from π to π^* states, which shifts to lower energies with increasing nitrogen incorporation. π-π^* transitions are much more probable than transitions from dangling bond states to the π^* states, because π and π^* states are localized at the same site and, thus, the optical matrix element is large. The optical absorption coefficient α can be approximated using Gaussian distributions D_π and D_{π^*} for the localized π and π^* bands, centered at E_π and E_{π^*} and with halfwidth $2w$:

$$D_{\pi,\pi^*}(E) = \frac{C}{w\sqrt{2\pi}} \exp\left[-\frac{(E - E_{\pi,\pi^*})^2}{2w^2} \right], \tag{1}$$

where C is proportional to the number of π and π^* states. If both bands are placed symmetrically around the Fermi energy, the absorption coefficient α can be written as

$$\alpha(E) \approx \frac{D}{E} \exp\left[-\frac{[E - (E_{\pi^*} - E_\pi)]^2}{4w^2} \right]. \tag{2}$$

The resulting joint density is again a Gaussian distribution. The prefactor D contains implicit information about the number of states ($\propto C^2$) and the optical matrix element. The fitting curves (solid lines) in Fig. 1(b) are calculated using Eq. (2), and confirm that nitrogen incorporation leads to a broadening of the π and π^* bands and, on the other hand, to a reduction of the pseudogap $E_{\pi\pi^*}=E_{\pi^*}-E_\pi$. For instance, comparing samples R0 (0% N_2) and R5 (5% N_2), the fitting of the experimental curve shows a decrease of $E_{\pi\pi^*}$ from 2.5 to 2.1 eV, as well as an increase of w from 0.4 to 0.53 eV as a result of the incorporation of nitrogen. In addition, the prefactor D increases as N_2 is incorporated by a factor of 5.

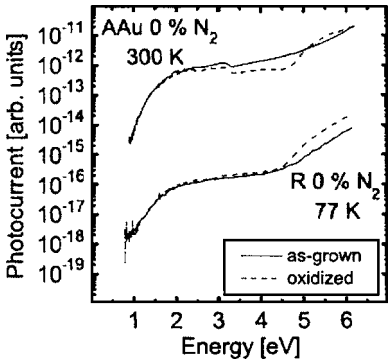

FIG. 2. Spectrally resolved photoconductivity of samples R0 and AAu, measured as grown (solid lines) and after oxidation (dashed lines). The absorption of surface states in the case of the as-grown sample masks the onset at higher energies, attributed to transitions from the valence band tail to the conduction band tail.

Figure 2 shows the SPC spectra of the undoped samples AAu and R0, measured as grown (solid lines) and after oxidation (dashed lines) in a conventional O_2 plasma. No change of dark conductivity was observed upon oxidation. Oxidation of the sample surface removes preferentially non-diamond (sp^2 bonded) regions from the surface. The initial rise of the photocurrent at 0.8 eV is again ascribed to the transition between π and π^*, as in PDS [see Fig. 1(b)]. A second onset at about 4.4 eV becomes more pronounced after the oxidation treatment. It is attributed to transitions from the valence band tail to the conduction band tail [Σ-Σ^* transitions in Fig. 1(a)]. The nature of the defect responsible for the photocurrent quenching at about 3.1 eV is unclear yet. However, the energy position suggests that it might be related to the optical defect center $H13$, a vacancy defect related with substitutional nitrogen, NV center, in the diamond grains.[8] Photons with sufficient energy can excite an electron to the defect level. The corresponding hole can tunnel to the grain boundary region where it can annihilate free carriers. Preliminary room temperature PL experiments evidenced the presence of NV centers in these films.[9] The incorporation of nitrogen impurities in the undoped films can be explained by uncontrolled contamination in the gas phase. Nevertheless, a conclusive assignation of the photocurrent quenching is not possible so far.

Figure 3(a) shows the temperature dependence of the spectrally resolved photoconductivity of sample AAu in the region between 3 and 6 eV. The onset of the quenching of the photoconductivity at 3.1 eV is shifted to lower energies with increasing temperature due to the reduction of the band gap with temperature. A shift of 0.2 eV is measured between 77 and 450 K, in good agreement with the expected shift of the band gap $dE_G/dT \approx -5\times10^{-4}$ eV/K.[10] Photothermal ionization processes to the conduction band tail can explain the shift of the onset at 4.4 eV to lower energies, as well as

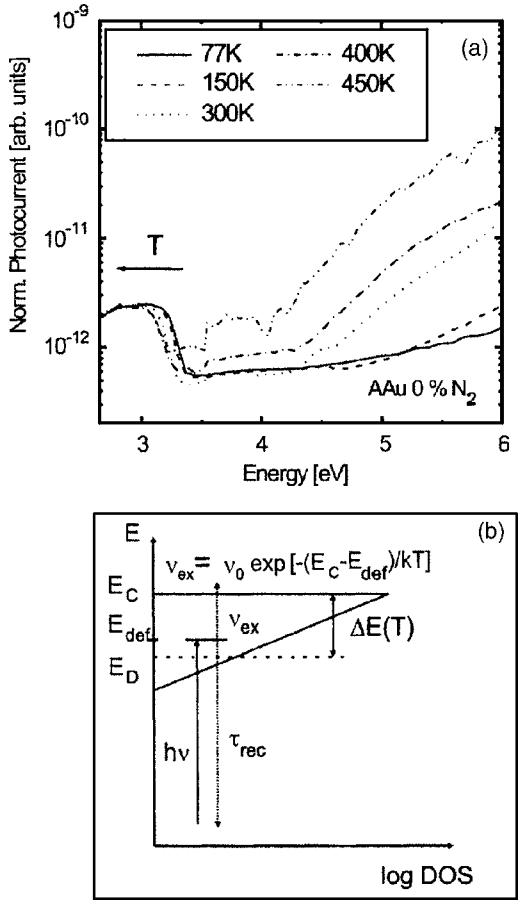

FIG. 3. (a) Temperature dependence of the spectrally resolved photoconductivity of sample AAu. The onset of the quenching of the photoconductivity is shifted to lower energies with increasing temperature. The intensity of photoconductivity at higher energies increases with temperature. (b) Schematic diagram of the density of states, assuming an exponential conduction bandtail.

the increase of the intensity of photocurrent at higher energies with temperature. Optical transitions into localized states of the bandtail [Fig. 3(b)] can contribute to the photoconductivity if the thermal excitation rate $\nu_{ex}=\nu_0 \exp[-(E_C - E_{def})/kT]$ is higher than the recombination rate τ_{rec}^{-1}, thus, $\tau_{rec}\nu_{ex} \geqslant 1$. E_C denotes the mobility edge of the conduction band, and E_{def} is the energy of the defect level in the bandtail. All transitions to defect levels above the demarcation energy $E_D=E_C-\Delta E$, obtained from $\tau_{rec}\nu_{ex}=1$, contribute to the photocurrent. Assuming typical values $\tau_{rec}\approx 10^{-9}$ s and $\nu_0 \approx 10^{14}\ s^{-1}$, one can estimate $\Delta E(450\ K)-\Delta E(77\ K) \approx 0.4$ eV, in good agreement with our results. The large increase in photocurrent with increasing temperature observed in Fig. 3, is correlated with the large increase of $N(\Delta E)$, which is the number of defect states lying between E_D and E_C:

$$N(\Delta E) = \int_{E_C-\Delta E}^{E_C} D(E)dE, \tag{3}$$

where $D(E)$ is the density of states.

In summary, PDS and SPC experiments have been applied to obtain complementary information about the subband gap structure of nanocrystalline diamond and about the influence of nitrogen incorporation. sp^2-bonded grain boundary atoms introduce π and π^* states into the band gap. Nitrogen incorporation entails an increase and broadening of the π and π^* bands. Comparison of optical absorption for both types of nanocrystalline diamond indicate similarities in the electronic band structure, and, thus, the existence of a common, well-defined nanocrystalline diamond phase.

Partially supported by Nano Diamond Network (NaDiNe) of the Austrian NANO initiative and by DRIVE (Diamond Research on Interfaces and Versatile Electronics) Marie Curie Research Training Network.

[1] D. M. Gruen, Annu. Rev. Mater. Sci. **29**, 211 (1999).
[2] A. R. Krauss, O. Auciello, D. M. Gruen, A. Jayatissa, A. Sumant, J. Tucek, D. C. Mancini, N. Moldovan, A. Erdemir, D. Ersoy, M. N. Gardos, H. G. Busmann, E. M. Meyer, and M. Q. Ding, Diamond Relat. Mater. **10**, 1952 (2001).
[3] K. Bakowicz and S. Mitura, J. Wide Bandgap Mater. **9**, 261 (2002).
[4] P. Zapol, M. Sternberg, L. A. Curtiss, T. Frauenheim, and D. M. Gruen, Phys. Rev. B **65**, 045403 (2001).
[5] S. Bhattacharyya, Phys. Rev. B **70**, 125412 (2004).
[6] J. Robertson and E. P. O'Reilly, Phys. Rev. B **35**, 2946 (1987).
[7] M. Nesladek, K. Meykens, L. M. Stals, M. Vanecek, and J. Rosa, Phys. Rev. B **54**, 5552 (1996).
[8] C. D. Clark, R. Ditchburn, and H. Dyer, Proc. R. Soc. London **237**, 75 (1956).
[9] F. Jelezko and J. Wrachtrup, (private communication).
[10] C. D. Clark, P. J. Dean, and P. V. Harris, Proc. R. Soc. London **277**, 312 (1964).